Deformation and crystallization of Zr-based amorphous alloys in homogeneous flow regime

Min Tao[a)]
Intel Corporation, Chandler, Arizona 85226

Atul H. Chokshi
Department of Metallurgy, Indian Institute of Science, Bangalore 560012, India

Robert D. Conner
Department of Manufacturing Systems Engineering and Management, California State University–Northridge, Northridge, California 91330

Guruswami Ravichandran
Graduate Aerospace Laboratories, California Institute of Technology, Pasadena, California 91125

William L. Johnson
Keck Laboratories of Material Science, California Institute of Technology, Pasadena, California 91125

(Received 11 July 2009; accepted 4 January 2010)

The purpose of this study is to experimentally investigate the interaction of inelastic deformation and microstructural changes of two Zr-based bulk metallic glasses (BMGs): $Zr_{41.25}Ti_{13.75}Cu_{12.5}Ni_{10}Be_{22.5}$ (commercially designated as Vitreloy 1 or Vit1) and $Zr_{46.75}Ti_{8.25}Cu_{7.5}Ni_{10}Be_{27.5}$ (Vitreloy 4, Vit4). High-temperature uniaxial compression tests were performed on the two Zr alloys at various strain rates, followed by structural characterization using differential scanning calorimetry (DSC) and transmission electron microscopy (TEM). Two distinct modes of mechanically induced atomic disordering in the two alloys were observed, with Vit1 featuring clear phase separation and crystallization after deformation as observed with TEM, while Vit4 showing only structural relaxation with no crystallization. The influence of the structural changes on the mechanical behaviors of the two materials was further investigated by jump-in-strain-rate tests, and flow softening was observed in Vit4. A free volume theory was applied to explain the deformation behaviors, and the activation volumes were calculated for both alloys.

I. INTRODUCTION

The inelastic deformation of bulk metallic glass[1,2] is fundamentally different from that of crystalline solids because of the lack of long-range order in the atomistic structures. It is a complicated process with intrinsic structural instability of the material and the interaction between its thermomechanical behavior and microstructural changes. Based on extensive experimental results for a wide range of metallic glasses including Zr-based alloys,[3–5] La-based alloys,[6,7] Fe-based alloys,[8,9] and Pd-based alloys,[10–12] three distinctly different deformation modes can be observed and described using their empirical flow characteristics: shear localization, occurring at room temperature and with high strain rate and featuring limited plasticity accumulated in localized thin shear bands; non-Newtonian flow, occurring at some moderate temperature in the vicinity of glass transition temperature (T_g) of the material and featuring stress over- and undershooting before steady-state stress is reached; and Newtonian flow, occurring in supercooled liquid regime of the material (above T_g and below crystallization temperature T_x) and featuring steady-state flow once yield starts. The first mode (shear localization) is an inhomogeneous flow mode, whereas the last two (non-Newtonian and Newtonian flow) are homogeneous flow modes. A recent review by Schuh et al.[13] summarizes the work and theories developed in field of homogeneous and inhomogeneous deformation of BMG.

There exist a number of theories describing the deformation mechanism of metallic glasses, such as the diffuse shear transformation and dislocation loop formation theory developed by Argon and coworkers,[14,15] the fictive stress model proposed by Kato et al.,[16] the directional structural relaxation model suggested by Khonik,[17] and the more recent cooperative shear model (CSM) developed by Johnson and coworkers[18–21] with the capability of predicting the temperature-dependent critical shear stress of bulk metallic glasses based on the potential energy landscape of the material. To associate

[a)]Address all correspondence to this author.
e-mail: min.tao@intel.com
DOI: 10.1557/JMR.2010.0134

the microstructural change of an amorphous alloy with its flow behavior, the free volume model developed by Spaepen and Turnbull[22] is still the most widely adopted theory that provides expressions for flow stress and strain rate as a function of defect concentration and temperature. Duine et al. used the free volume based viscosity and defect evolution assumption by Spaepen to analyze the kinetic process of defects and their steady-state concentration.[23] de Hey et al. applied the same idea to temperature-induced structural evolution of some metallic glasses, leading to the conclusion that additional free volume was created compared with thermal equilibrium due to plastic deformation.[7,24] Adopting the free volume concept, Anand and Su extended their elastic-viscoplastic constitutive model[25] for metallic glass deformed at room temperature to high temperature homogenous flow regime[26] and applied it to capture the stress over- and undershort phenomena in non-Newtonian flow observed in earlier experiments.[24]

The recent developments in technology have provided advanced tools to experimentally study the complicated phenomena associated with crystallization and structural relaxation in BMGs at the microstructural level resulting from thermal or mechanical loading. Waniuk et al. studied a series of bulk Zr–Ti–Ni–Cu–Be amorphous alloys using differential scanning calorimetry (DSC) and x-ray diffraction to understand how changes in isothermal annealing temperature and annealing time affected the volume fraction of crystallization and shift in T_g.[27] Transmission electron microscopy (TEM) and small-angle neutron scattering (SANS) techniques were applied to study in detail the crystallite microstructure formed in Zr-based BMGs during annealing.[28] After Chen et al.[29] first reported the formation of nanocrystallites in the shear bands of amorphous Al-based alloys observed with TEM, there has been much experimental evidence for nanoscale crystallites formed in the vicinity of shear bands, fracture surfaces, nanoindentation, and in tensile and bending tests at room temperature or below.[30–32] In the homogeneous flow region, de Hey et al. further associated the glass transition behavior in the DSC trace of the deformed specimen with the amount of free volume and used it to explain the deformation behavior of Pd- and La-based alloys.[7,23,24] Heggen et al. used compression creep testing at constant stress and during jump stress to study the structural relaxation and disordering during the high-temperature deformation of a Pd–Ni–Cu–P alloy, from the perspective of free volume creation and annihilation.[33,34] Nieh et al. suggested nanocrystallization in the amorphous structure during the homogeneous deformation based on x-ray diffraction and TEM examinations of the superplastically deformed specimens.[4,35,36] A group of researchers also reported observation of spinodal decomposition or phase separation preceding nanocrystallization, shown as a separate initial crystallization portion prior to the primary crystallization event in DSC traces.[37–39]

The purpose of this study is to experimentally investigate the interaction of inelastic deformation and the microstructural changes such as decomposition and nanocrystallization of two Zr-based amorphous alloys using high-temperature compression tests coupled with DSC and TEM examination to further understand the fundamental deformation mechanisms of the BMGs in their supercooled liquid regions.

Two structural amorphous alloys, $Zr_{41.25}Ti_{13.75}Cu_{12.5}Ni_{10}Be_{22.5}$ (Vitreloy 1) and $Zr_{46.75}Ti_{8.25}Cu_{7.5}Ni_{10}Be_{27.5}$ (Vitreloy 4), were chosen for this study. Among the best glass-forming alloys with the most promising structural application, the two Vitreloy alloys have been well studied in their physical properties. After Vitreloy 1 was first discovered in 1993 at Caltech,[40] extensive studies have been carried out to evaluate the thermodynamic and rheological properties of the material.[38,41] The deformation behavior of Vitreloy 1 across a wide range of temperatures and strain rates have been studied by Lu et al. using compression testing.[3] The viscosity of Vitreloy 4 over the range between 10^5 and 10^9 Pa·s has been measured by Busch et al. using parallel plate rheometry and three-point beam bending.[42] Though both materials have similar compositions, glass-forming ability, and mechanical properties, they exhibit distinctly different thermal properties as shown by their DSC traces. One of the characteristics of the DSC curve of Vitreloy 1 (with heating rate of 20 K/min) is that the crystallization event occurs in two steps: an initial portion (which is referred to as a spinode) indicating phase separation before primary crystallization, followed by the primary crystallization. This feature is not found in the DSC curve of Vitreloy 4, which exhibits two clearly separated crystallization events, with a small secondary event following the primary crystallization. Previous research on the crystallization and decomposition behaviors of these two alloys and alloys of similar composition focused mostly on the thermal effects; little is known about the interplay between the microstructural changes and the mechanical properties of the two alloys, which is important in understanding the deformation mechanisms for the purpose of analyzing and designing thermomechanical processes and structural applications of these materials.

Uniaxial compression tests were performed on the two alloys at a fixed temperature in their supercooled liquid region at various strain rates, followed by characterization using DSC and TEM examination. The influence of the structural change on the mechanical behavior of the two amorphous alloys was studied using jump-in-strain-rate tests, performed independently in their non-Newtonian and Newtonian flow regions, and drop-in-strain-rate from non-Newtonian to Newtonian flow region.

II. EXPERIMENTAL

Liquid Metal Technologies, Inc. (Lake Forest, CA) provided a cast plate of Vitreloy 1, which was EDM cut into rectangular compression specimens with the dimensions 2.9 × 2.9 × 5.8 mm. DSC of the as-received material revealed that the onset of its glass transition temperature (T_g) was 623 K, and the onset of its crystallization temperature (T_x) was 712 K when heated at 20 K/min. The Vitreloy 4 samples were prepared from elemental metals of purity ranging from 99.9 to 99.999% by vacuum induction melting in a water-cooled copper hearth, followed by vacuum casting to form glassy rods of 3 mm in diameter and 25 mm in length. The rods were cut into specimens of 6 mm in length, with ends ground and polished perpendicular to the longitudinal axis. T_g and T_x of the as-cast material were measured using DSC to be 617 and 740.5 K, respectively, at a heating rate of 20 K/min. The top and bottom surfaces of all specimens were polished with 600-grit sandpaper. During the compression tests, high-temperature Bentone-Clay semi-synthetic grease was applied on both surfaces to reduce the effect of friction.

Quasi-static uniaxial compression tests were performed on a servohydraulic Materials Testing System (MTS 358 series) with a loading fixture built in-house for high-temperature compression. The test temperature was controlled at $T = 643 \pm 0.5$ K, a constant temperature within the supercooled liquid regimes of both materials ($T_g < T < T_x$). According to a previous study on the thermodynamic and kinetic properties of the two alloys,[26] their time–temperature–transformation (TTT) diagrams show that Vitreloy 1 has a time window of more than 3000 s before crystallization, while Vitreloy 4 requires more than 10,000 s to crystallize at this temperature, which provides ample time for the materials to reach steady-state flow under compressional loading without initiating crystallization from thermal effects alone. For consistency, the specimens were held at the testing temperature for up to 3 min to reach thermal equilibrium throughout the body before the loading started. Displacement-controlled compressive loading was performed, and the tested specimens were quenched in room-temperature water immediately after the loading was completed.

Compression tests at three constant strain rates on the order of 10^{-2}, 10^{-3}, and 10^{-4} s^{-1} were performed on both alloys. Two sets of jump-in-strain-rate tests were also conducted on each alloy. The first set consisted of single-rate-drop tests in which the strain rate dropped from a high strain rate $\dot{\varepsilon}_h$ to a low strain rate $\dot{\varepsilon}_1$ ($\dot{\varepsilon}_1/\dot{\varepsilon}_h < 0.01$), corresponding to a change in flow from the non-Newtonian to Newtonian mode. The results of the constant-strain-rate tests at $\dot{\varepsilon}_1$ and $\dot{\varepsilon}_h$ were compared with the results of the jump-in-strain-rate tests. The second set consisted of compression tests performed with multiple strain-rate-dropping within the non-Newtonian regime and within the Newtonian region, independently. In the non-Newtonian strain rate jump test, attention was paid to ensure that the flow reached steady state at each step before jumping to a lower strain rate.

All constant-strain-rate tests were performed in the homogeneous flow region for both materials, and it was reasonable to assume that small pieces of material (~15 mg each) cut from each specimen for DSC and TEM examination represented the thermal properties of the entire specimen. A Netzsch 404 C DSC analyzer (Selb, Germany) in the Keck Materials Research Laboratory of Caltech was used in the current investigation. DSC control samples of Vitreloy 1 and Vitreloy 4 were prepared with the same thermal history as those specimens that experienced the longest testing time, i.e., a heating time of ~25 min and holding time of ~20 min at the desired testing temperature. Thus, by comparing the DSC results of the deformed (tested) specimen and the control sample, the effect of mechanical deformation on the decomposition, and nanocrystallization of the alloy could be distinguished from the changes caused by the thermal effect alone. TEM specimens were prepared by ultramicrotome and examined using a Philips EM420 (Eindhoven, The Netherlands) at an accelerating voltage of 120 kV. An identical process was applied in preparing both Vitreloy 1 and Vitreloy 4 samples, and caution was taken to minimize the sample preparation interference with the crystalline characteristics of the samples. Finally, to confirm the crystallization characteristics revealed by TEM, x-ray diffraction spectra were performed on both tested Vitreloy 1 and Vitreloy 4 samples using a Philips X'pert Pro diffractometer (PANalytical B.V., Almelo, The Netherlands).

III. RESULTS

A. Stress-strain response of constant strain rate tests

The true stress–strain curves obtained in uniaxial compression for Vitreloy 1 and Vitreloy 4 deformed at $T = 643$ K are shown in Fig. 1 for a variety of constant strain rates.

As illustrated in Figs. 1(a) and 1(b), the stress–strain behavior of both alloys is highly strain-rate sensitive at 643 K, and a trend from non-Newtonian to Newtonian flow mode can be observed with decreasing strain rate. The non-Newtonian flow features of stress overshoot and undershoot are observed in the Vitreloy 1 tests at $\dot{\varepsilon} = 0.04$ s^{-1} and $\dot{\varepsilon} = 0.003$ s^{-1}, as well as in the Vitreloy 4 tests at $\dot{\varepsilon} = 0.05$ s^{-1} and $\dot{\varepsilon} = 0.004$ s^{-1}. The Vitreloy 1 specimen tested at $\dot{\varepsilon} = 3 \times 10^{-4}$ s^{-1} and the Vitreloy 4 specimen tested at $\dot{\varepsilon} = 5 \times 10^{-4}$ s^{-1} are in the Newtonian flow mode, reaching steady-state flow without either over- or undershooting. The slight increase in flow stress at large strains

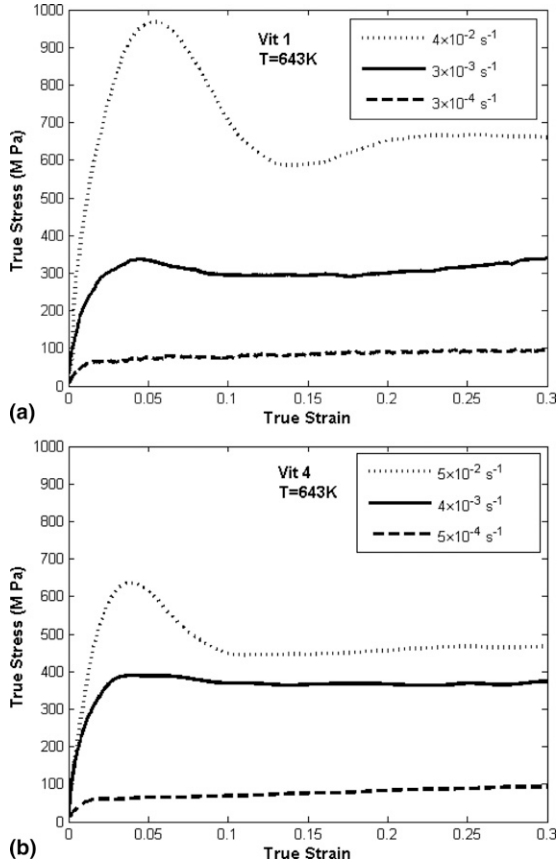

FIG. 1. True stress–strain curves from compression tests performed at 643 K and various strain rates: (a) Vitreloy 1, $\dot{\varepsilon} = 0.04\ s^{-1}$, $\dot{\varepsilon} = 0.003\ s^{-1}$, and $\dot{\varepsilon} = 3 \times 10^{-4}\ s^{-1}$; (b) Vitreloy 4, $\dot{\varepsilon} = 0.05\ s^{-1}$, $\dot{\varepsilon} = 0.004\ s^{-1}$, and $\dot{\varepsilon} = 5 \times 10^{-4}\ s^{-1}$.

in the Newtonian regime is related to the large strain rate sensitivity of flow and the increase in strain rate in compression tests performed at constant displacement rates.

B. DSC results

The specimens deformed in compression at different strain rates and jump-in-strain-rate were examined by DSC, along with the two control samples described earlier, at a constant heating rate of 20 K/min. The following important features on the DSC traces of these specimens were examined: (i) the shift in the onset of the glass transition temperature, T_g, and the change in the supercooled liquid region, $\Delta T = T_x - T_g$; (ii) the change in the specific heat capacity, c_p, at the glass transition temperature; (iii) enthalpy change during the crystallization event(s), i.e., $\Delta H_{cryl} = \int \Delta c_p dT$, where the subscript "cryl" designates crystallization; and (iv) the characteristics of the crystallization event(s). Lower T_g and larger ΔT are believed to be associated with increased thermal stability and better glass formability.[26] The specific heat change at the glass transition region has been considered an important feature in the studies of the thermophysical

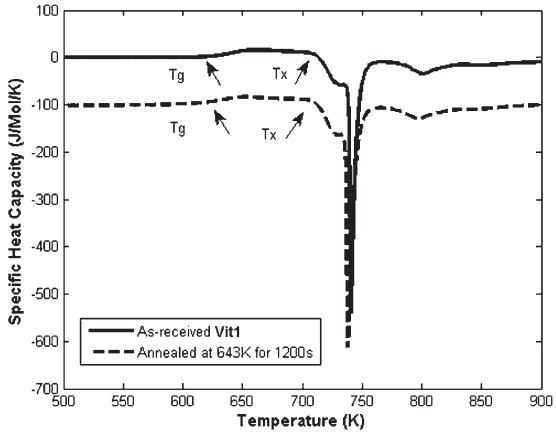

FIG. 2. DSC traces of Vitreloy 1 control test sample compared to that of the as-received sample. The annealing time for the control sample represented the longest testing time of Vitreloy 1 in this investigation. The DSC curves are shifted relative to one another along the ordinate for display purposes.

properties of amorphous materials. Some investigators believe it to be direct evidence of free volume concentration in the material at the beginning of the DSC scans.[7,23,24] Such a hypothesis provides a good explanation for the present results, which is discussed later. By comparing the enthalpy change during the crystallization process of the deformed (designated by the subscript "def") samples and that of the as-cast (designated by the superscript "a-c") sample, the fraction of crystallization in the materials can be estimated as

$$f_{cryl} = (\Delta H^{a\text{-}c}_{cryl} - \Delta H^{def}_{cryl})/\Delta H^{a\text{-}c}_{cryl} \quad .$$

The change in the shape of the initial portion of the crystallization curve (spinode) for Vitreloy 1 before the primary crystallization is an indication of intrinsic phase separation that serves as the nucleation source for subsequent crystallization.[37,38]

DSC traces of the as-received sample and a control sample of Vitreloy 1 are both shown in Fig. 2, and they are almost identical. Because the two samples have the same thermal histories, the effect of heating alone on the phase change can thus be excluded from all the Vitreloy 1 specimens in this investigation that are tested at temperature $T = 643$ K within the specified time range.

DSC traces of Vitreloy 1 specimens deformed at constant strain rates are shown in Fig. 3, and the results are summarized in Table I. With decreasing strain rate, T_g decreases and the span of supercooled liquid region ΔT decreases (see Table I). This indicates that the material is less thermally stable following mechanical deformation in the supercooled liquid region than the as-received material. It was hard to determine the fractions of crystallization of Vitreloy 1 samples accurately on the DSC analyzer based on enthalpy change during the primary crystallization process, because the primary crystallization

event in Vitreloy 1 overlapped the spinal nucleation precursor and could not be separated out for the enthalpy calculation. However, it is clear from Fig. 3 that with decreasing strain rate, the enthalpy change in the spinodal nucleation part increases and that in the primary crystallization part reduces. The amplitude of the peak corresponding to spinodal phase separation nearly doubles in the deformed material compared with that of the as-received material and the control sample. This implies crystal formation during thermomechanical loading in the high-temperature compression test. The crystals that form at the spinode serve as nuclei for further crystallization, and a larger fraction of material is crystallized during tests at the lower strain rates. This observation is further validated through TEM examination as discussed in Sec. III. C.

The DSC results of as-received, tested, and control samples of Vitreloy 4 are shown in Figs. 4 and 5, and the associated values inferred from the traces are tabulated in Table II. From Fig. 4, the computed integrated area of the specific heat capacity over the temperature duration of the crystallization event(s) remains almost the same for the control sample and the as-received material; i.e., $f_{\mathrm{cryl}} \approx 0$, and the material remains amorphous after annealing. However, instead of crystallizing in two separate events such as the as-received material, the control sample, subjected to pure thermal loading, crystallizes in a single event at a lower T_{x}. The phenomenon of the merging of the two separate crystallization events into one was also observed in isothermal crystallization at higher temperatures of other alloys in

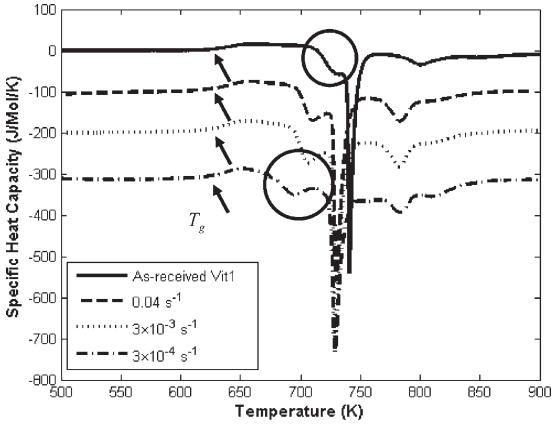

FIG. 3. DSC traces of deformed Vitreloy 1 specimens compared with that of the as-received sample. The DSC curves are shifted relative to each other along the ordinate for display purposes. The amplitude of phase-separation spinode (as circled out in the figure) increases after mechanical deformation.

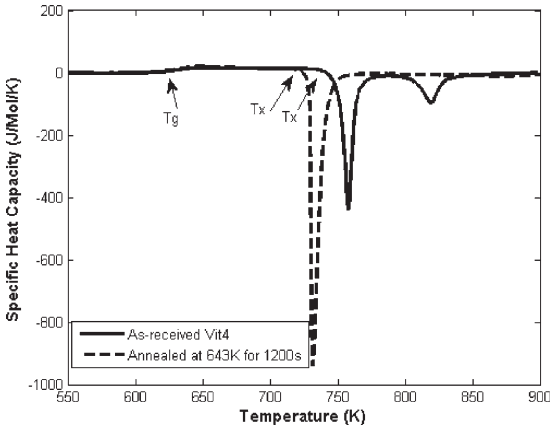

FIG. 4. DSC traces of Vitreloy 4 control test sample compared with that of the as-received material. The annealing time of the control sample represented the longest testing time of Vitreloy 4 during compressive loading.

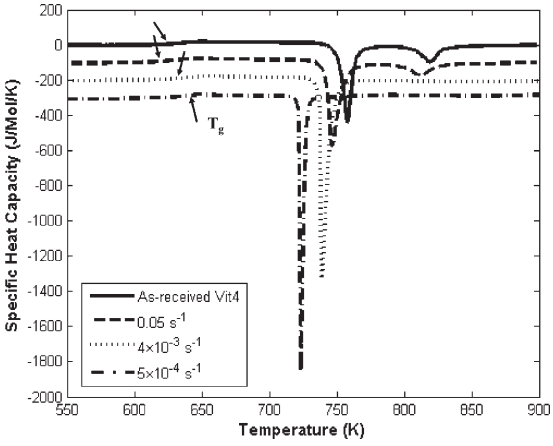

FIG. 5. DSC traces of the deformed Vitreloy 4 specimens compared with that of the as-received material. The DSC curves are shifted relative to each other along the ordinate for display purposes.

TABLE I. Summary of the DSC results for Vitreloy 1.

	As-received sample	Control sample	$\dot{\varepsilon} = 0.04\ \mathrm{s}^{-1}$	$\dot{\varepsilon} = 0.003\ \mathrm{s}^{-1}$	$\dot{\varepsilon} = 3 \times 10^{-4}\ \mathrm{s}^{-1}$
T_{g} (K)	622.8	622.8	622.6	620.0	619.8
$\Delta T = T_{\mathrm{x}} - T_{\mathrm{g}}$ (K)	89.6	88.7	74.4	73.1	65.2
Spinodal phase separation	...	Advanced by ~6 K; almost no change in peak amplitude and shape	Advanced by 15.7 K; peak increased by about twice in amplitude	Advanced by 19.3 K; peak increased by about twice in amplitude	Advanced by 27.4 K; peak increased by about twice in amplitude

TABLE II. Summary of the DSC results for Vitreloy 4.

	As-received sample	Control sample	$\dot{\varepsilon} =$ 0.05 s^{-1}	$\dot{\varepsilon} =$ 0.004 s^{-1}	$\dot{\varepsilon} = 5 \times 10^{-4}$ s^{-1}
T_g (K)	616.9	616.5	611.3	621.1	631.3
$\Delta T = T_x - T_g$ (K)	123.6	105.5	133.7	106.6	96.2
f_{cryl}	...	~0	~0	~0	~0
Secondary crystallization	Yes	No	Yes	No	No

the Vitreloy family, which was attributed to the kinetic nature of nucleation.[27]

As shown in Fig. 5, the secondary crystallization event for compression samples disappears for all Vitreloy 4 specimens except for the one deformed at $\dot{\varepsilon} = 0.05$ s^{-1}, which still shows a small secondary crystallization event. The glass transition temperature, T_g, decreases with lower strain rate and longer testing time, same as the observation from Vitreloy 1. The onset temperature of rapid primary crystallization also tends to decrease with decreasing strain rate; e.g., T_x of the specimen after testing at $\dot{\varepsilon} = 5 \times 10^{-4}$ s^{-1} is approximately 10 K lower than that of the as-received material. It is worth noting that the crystallization peak is sharper for samples deformed at lower strain rates even though $f_{cryl} \approx 0$. This will also be validated by TEM images in Sec. III. C. The change in kinetic behavior of crystallization during thermal analysis may be explained by local decomposition from varying thermomechanical loading conditions. Such strain-rate-induced composition fluctuation is usually too small to be detectable with microprobe or microscopy techniques,[43] but may lend itself to study using techniques with higher resolution, such as small-angle neutron scattering.[28]

C. TEM and x-ray results

Samples of Vitreloy 1 and Vitreloy 4 tested at strain rates spanning from 10^{-2} to 10^{-4} s^{-1} were examined using TEM. Figure 6 shows the microstructures and diffraction patterns of Vitreloy 1 [Fig. 6(a)] and Vitreloy 4 [Fig. 6(b)] samples after compression test in Newtonian region at strain rates of 4×10^{-3} s^{-1} and 5×10^{-4} s^{-1}, respectively. Crystallization in Vitreloy 1 is revealed by the bright spots embedded in the amorphous halo in the diffraction pattern inset in Fig. 6(a), taken from the region shown in the associated bright-field image. Vitreloy 4 remains amorphous after the compression test, with no crystals in the diffraction pattern or the bright-field image. In fact, in this study, Vitreloy 1 shows crystallization as a result of deformation at all strain rates, while Vitreloy 4 shows none. The results are consistent with the observation from their DSC curves described in Sec. III. B. For Vitreloy 1, nanocrystallines are accumulated under mechanical load

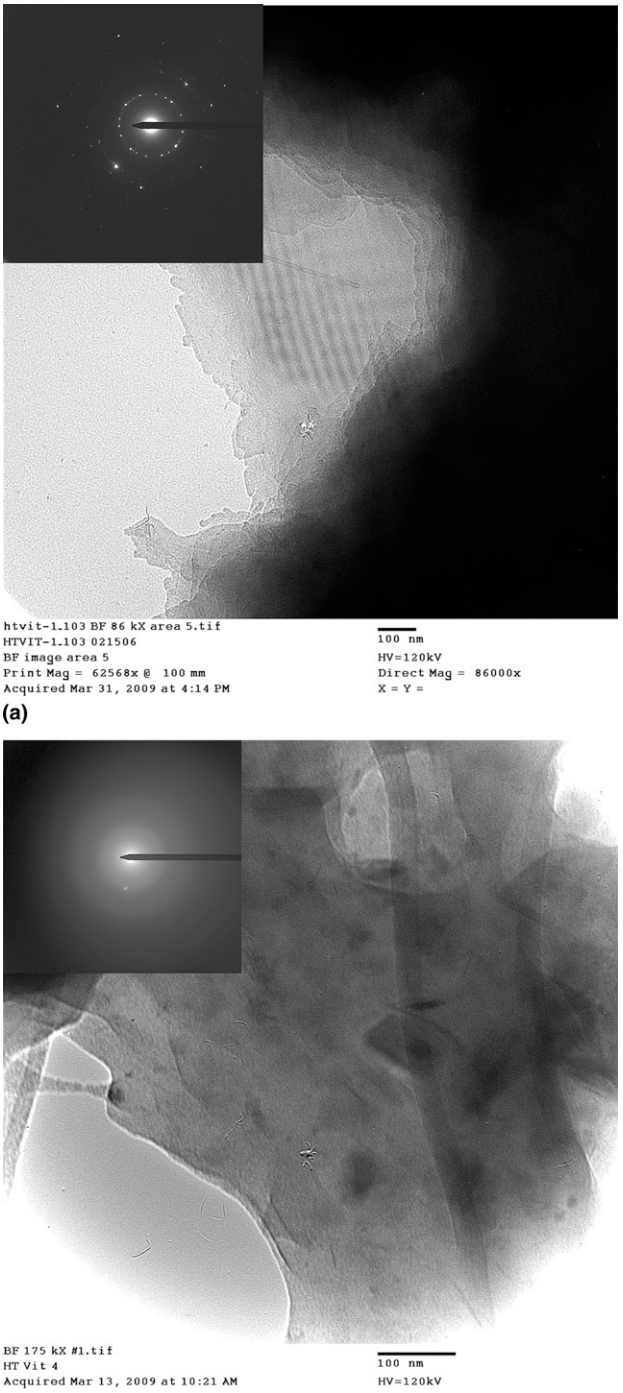

FIG. 6. Transmission electron images of two alloys after low strain rate compression test: (a) Bright-field image of Vitreloy 1 tested at $\dot{\varepsilon} = 4 \times 10^{-3}$ s^{-1} showing sharp amorphous/crystallite interface, with crystalline diffraction pattern in the inset; (b) Vitreloy 4 tested at $\dot{\varepsilon} = 5 \times 10^{-4}$ s^{-1} showing no clear crystallite boundary, with amorphous diffraction pattern in the inset.

through the spinodal separation event prior to the main crystallization, and the enthalpy change during the primary crystallization event reduces as an indication of partial crystallization of the sample (Fig. 3). On the

other hand, the enthalpy change during DSC measurement for Vitreloy 4 does not show much crystallization (Table II), and the DSC curves of samples after thermomechanical loading demonstrate totally amorphous characteristics, with changes only in atomistic disordering behaviors (Fig. 5). A previous in situ TEM annealing experiment on a Zr-based BMG also showed annealing at temperature above its T_g could cause compositional fluctuation without introducing electron diffraction pattern change, as what was discovered here on Vit4 under thermal mechanical loading.[44]

To validate the difference in the thermomechanical deformation induced crystallization behavior of the two alloys, x-ray diffraction spectra of the two test samples in Fig. 6 were collected using a Philips X'pert Pro diffractometer. The diffraction spectra are shown in Fig. 7. The curve on the top showing crystallization embedded in the amorphous matrix is Vitreloy 1 sample tested at strain rate of 4×10^{-3} s^{-1}, with corresponding TEM images in Fig. 6(a). The smooth curve on the bottom showing entirely amorphous phase is Vitreloy 4 sample tested at strain rate of 5×10^{-4} s^{-1}, with corresponding TEM images in Fig. 6(b). The signal from Vitreloy 4 is weaker due to smaller sample size.

The x-ray diffraction peaks of the Vitreloy 1 sample analyzed using Philips X-Pert software with x-ray data generated via Cu Kα radiation were labeled in Fig. 7. According to work published by Martin et al.,[45] the crystallization path for Vitreloy 1 is: amorphous → amorphous + i-phase → Be_2Zr + $CuZr_2$ + unidentified phase. Other authors, e.g., Nieh et al.,[46] writing on the crystallization behavior of similar but different Zr-based BMG systems also identified the formation of $Ni_{10}ZR_7$ and $Cu_{10}Zr_7$ compounds upon crystallization. Results of x-ray analysis here show that, for the Vitreloy 1 sample tested at strain rate of 4×10^{-3} s^{-1}, $Ni_{10}Zr_7$ is present at the first and third peaks, $Cu_{10}Zr_7$ is present at the first peak, $NiZr_2$ is present at the second peak, and $CuZr_2$ is present at the third peak. Data for peak locations for $NiZr_2$ and $CuZr_2$ were taken from the work of Fatay et al.,[47] as these data were not available in the Philips X-Pert database.

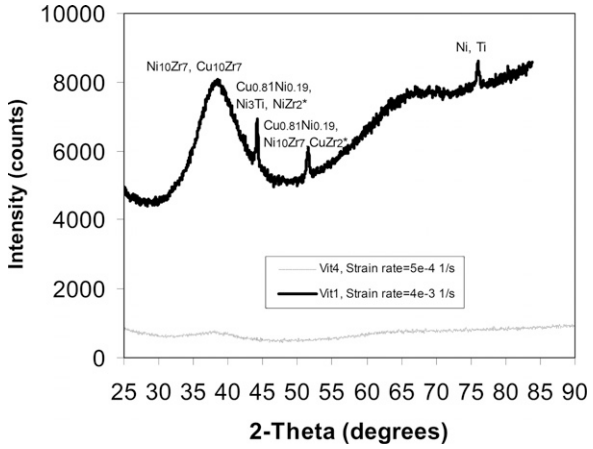

FIG. 7. X-ray diffraction spectra of Vitreloy 1 tested at $\dot{\varepsilon} = 4 \times 10^{-3}$ s^{-1} (top curve with crystalline breakouts) and Vitreloy 4 tested at $\dot{\varepsilon} = 5 \times 10^{-4}$ s^{-1} (smooth curve). Crystalline peaks in the Vitreloy 1 curve were indexed using the database with the Philips X-Pert software and crystals marked with * were from Ref. 48.

D. Jump-in-strain-rate tests

To understand the influence of the structural changes on the mechanical behavior of the two alloys, single jump-in-strain-rate tests and successive jump-in-strain-rate tests were performed on both Vitreloy 1 and Vitreloy 4. Single jump-in-strain-rate tests were compression tests conducted by dropping the strain rate to the Newtonian regime after having reached the steady-state flow in the non-Newtonian flow regime. The true stress–strain curves are compared with those of the corresponding constant strain rate compression tests in Fig. 8. The two alloys exhibit distinct differences in terms of their flow

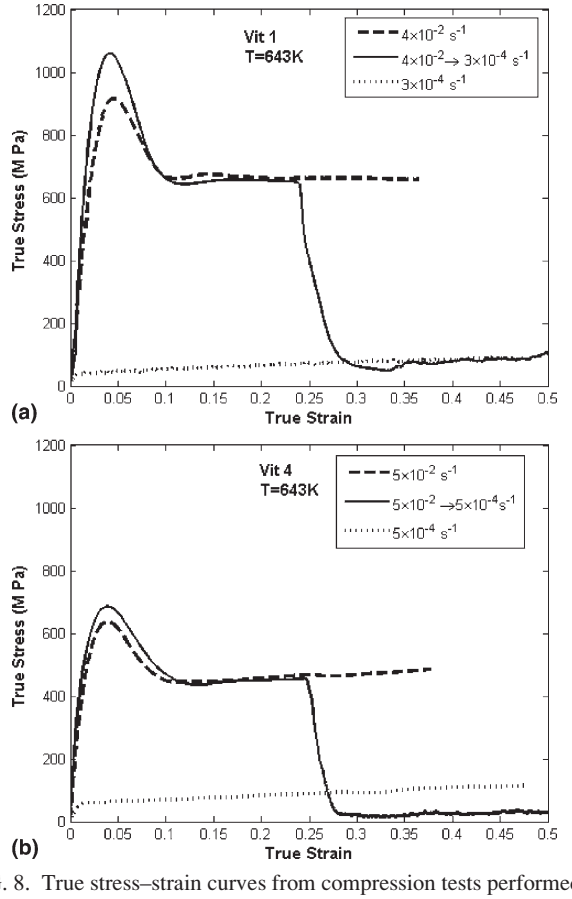

FIG. 8. True stress–strain curves from compression tests performed at 643 K at two constant strain rates (one in the non-Newtonian regime and another in the Newtonian regime) and jump (drop) in strain rate with mode of deformation going from non-Newtonian to Newtonian regime: (a) Vitreloy 1, $\dot{\varepsilon} = 0.04$ s^{-1}, $\dot{\varepsilon} = 3 \times 10^{-4}$ s^{-1}, and $\dot{\varepsilon} = 0.04 \rightarrow 3 \times 10^{-4}$ s^{-1}; (b) Vitreloy 4, $\dot{\varepsilon} = 0.05$ s^{-1}, $\dot{\varepsilon} = 5 \times 10^{-4}$ s^{-1}, and $\dot{\varepsilon} = 0.05 \rightarrow 5 \times 10^{-4}$ s^{-1}.

strength after the strain rate drop. For Vitreloy 1, consistent with observations in literatures,[3,48] the final steady-state flow stress in the rate jump is the same as that in the constant low rate test [Fig. 8(a)]. However, for Vitreloy 4, the flow stress after the rate drop is observed to be less than one-third of that of the constant rate test at the corresponding low strain rate [Fig. 8(b)].

Successive jump-in-strain-rate tests were performed by dropping the strain rates multiple times independently in both the non-Newtonian and Newtonian flow regions. In the non-Newtonian jump-in-strain-rate test, caution was taken to ensure that the flow had reached steady state at each step before jumping to a lower strain rate. The true stress–strain curves for the successive jump-in-strain-rate tests are plotted in Figs. 9(a) and 9(b) for Vitreloy 1 and Vitreloy 4, respectively. As expected, drops in flow stress are observed at each strain rate drop. Also shown in Fig. 8 are the free volumes calculated from the flow curves. The dependency of the steady-state flow stress on the strain rate in each test is plotted in Figs. 10(a)–10(d) along with predictions from the free volume model discussed in the next section.

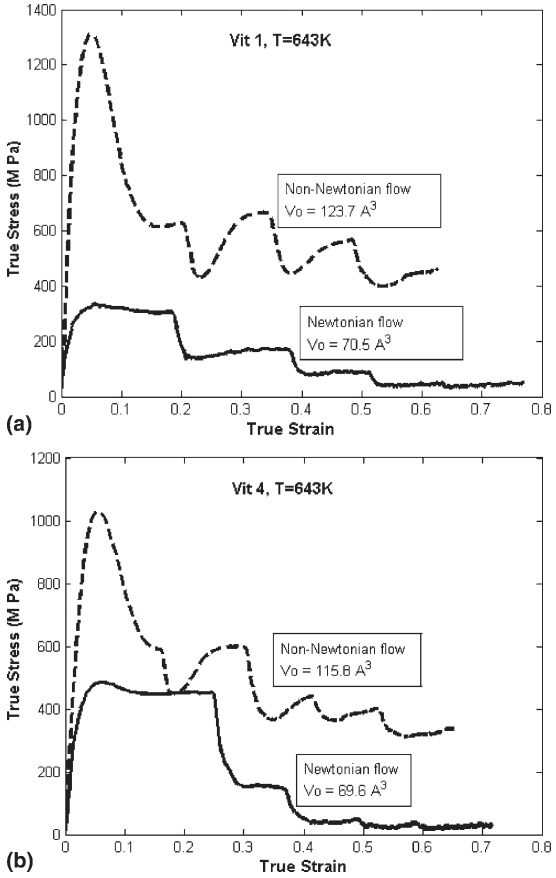

FIG. 9. True stress–strain curves for successive jump in strain rate tests of: (a) Vitreloy 1 deformed in the non-Newtonian flow region (dashed line) with the strain rate history of $\dot{\varepsilon} = 7.4 \times 10^{-2} \rightarrow 2.6 \times 10^{-2} \rightarrow 1.2 \times 10^{-2} \rightarrow 6.0 \times 10^{-3}$ s^{-1}, deformed in the Newtonian flow region (solid line) with the strain rate history of $\dot{\varepsilon} = 2.6 \times 10^{-3} \rightarrow 1.2 \times 10^{-3} \rightarrow 6.2 \times 10^{-4} \rightarrow 2.4 \times 10^{-4} \rightarrow 1.3 \times 10^{-4}$ s^{-1}; (b) Vitreloy 4, deformed in the non-Newtonian flow region (dashed line) with the strain rate history of $\dot{\varepsilon} = 6.8 \times 10^{-2} \rightarrow 3.4 \times 10^{-2} \rightarrow 1.2 \times 10^{-2} \rightarrow 8.9 \times 10^{-3} \rightarrow 6 \times 10^{-3}$ s^{-1}, deformed in the Newtonian flow region (solid line) with the strain rate history of $\dot{\varepsilon} = 1.7 \times 10^{-2} \rightarrow 3.5 \times 10^{-3} \rightarrow 1.3 \times 10^{-3} \rightarrow 4.3 \times 10^{-4} \rightarrow 1.9 \times 10^{-4}$ s^{-1}.

IV. DISCUSSION

A. Deformation-induced relaxation phenomena

Even though Vitreloy 1 and Vitreloy 4 have similar chemical compositions and both exhibit good glass formability and mechanical properties at room temperature, their high-temperature deformation behaviors are different, which can be attributed to the different relaxation mechanisms in the two nonequilibrium alloy systems.

DSC examination of the specimens following compressive deformation in their supercooled liquid regions suggests that the types of phase changes dominating the relaxation process are quite different in Vitreloy 1 and Vitreloy 4. For the as-received Vitreloy 1 material, the DSC trace at a constant heating rate of 20 K/min features a spinodal portion immediately after the glass transition and before the primary heat release, which indicates the existence of an initial crystallization process prior to the major crystallization event. The so-formed crystallites serve as the nuclei for further crystallization. Similar to the observation in this study, an annealing study on Vitreloy 1 conducted by Gao et al.[49] also reported that the spinodal portion starts to appear at temperatures above 793 K, which is lower than the crystallization temperature, and increases in magnitude and reduces in the incubation time with higher temperatures. They called this sequence a "multistage crystallization" and reported the formation of different phases during the different crystallization stages in TEM examination followed by the annealing. In situ small-angle-neutron-scanning performed by Loffler and Johnson[50] also supports the conclusion that as Vitreloy 1 relaxes it undergoes phase separation at the nanoscale followed by crystallization. In the present study, mechanically loading the supercooled liquid produces the same microstructural changes as the structural relaxation process of Vitreloy 1. The phase separation and nanocrystallization similar to the observation of Gao et al.[49] are triggered by the coupled thermal and mechanical driving forces instead of purely thermal effect that might occur at an even higher temperature in the homogeneous flow regime.

For Vitreloy 4, the DSC trace of the as-received material features two crystallization events, with a smaller secondary event following primary crystallization. It does not have the spinodal phase separation as observed in Vitreloy 1. The supercooled liquid regime of Vitreloy 4 ($\Delta T = 123$ K) is also larger than that of Vitreloy 1 ($\Delta T = 89$ K), which indicates Vitreloy 4 is more thermally stable than

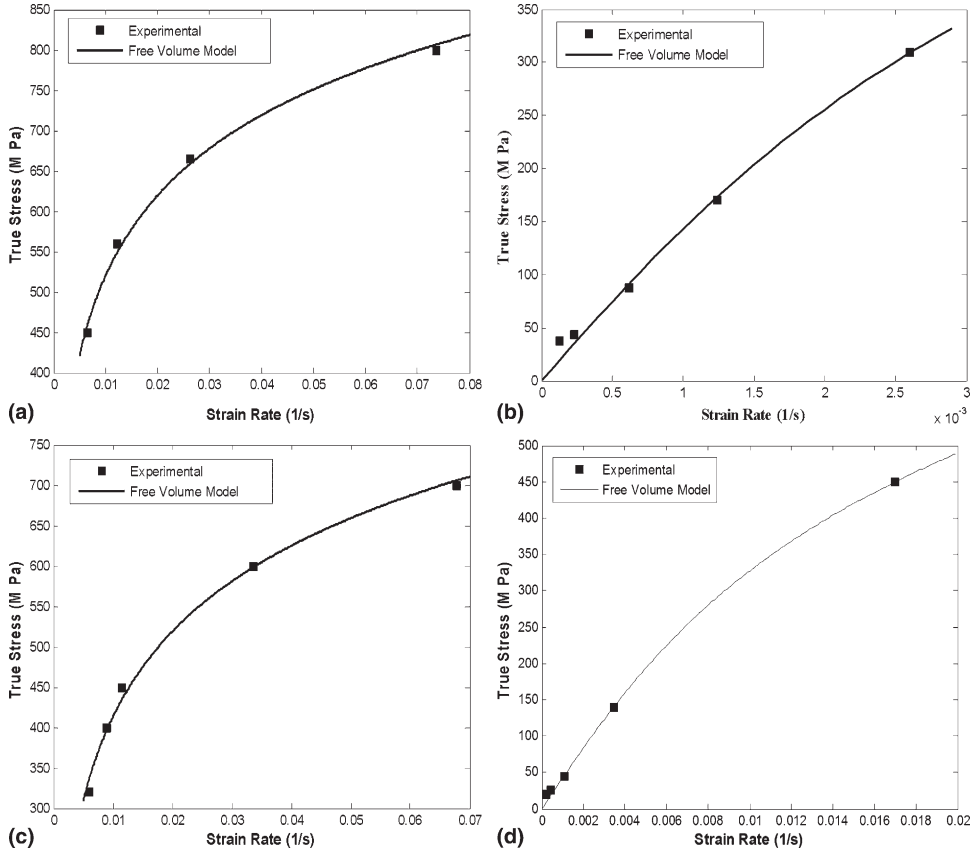

FIG. 10. Experimental and predicted strain-rate dependence of flow stress from multiple jump-in-strain-rate tests at 643 K. For Vitreloy 1: (a) in the non-Newtonian flow region and (b) in the Newtonian flow region. For Vitreloy 4: (c) in the non-Newtonian flow region and (d) in the Newtonian flow region. The solid lines are model predictions using Eq. (1). See Table III for the activation volume and prefactor in each case.

Vitreloy 1.[27] Indeed, no crystallite formation was found in the mechanically deformed Vitreloy 4 specimens by TEM and x-ray examination. The most evident phenomenon in the DSC traces of the deformed Vitreloy 4 specimens is that after the coupled thermal and mechanical loading, the two crystallization events converged to become a single sharp and abrupt peak. Lower strain rate, and therefore longer testing time, promotes such a tendency. The control specimen with the same thermal history as the specimen tested at low strain rate shows a similarly single major crystallization event in the DSC trace, but the crystallization peak is not as narrow as those found after mechanical deformation. This suggests that the relaxation process in Vitreloy 4 is driven by both mechanical and thermal effects. The integrated areas of the crystallization event(s), i.e., enthalpy released during the crystallization(s), remain essentially identical in all specimens, which suggests that the specimens are still entirely amorphous despite the change in character of the DSC traces. A similar phenomenon of merging of crystallization events was also observed by other researchers in isothermal calorimetrical study on Vitreloy 4.[27] Such a phenomenon is associated with the change of atomic mobility in the alloy system. Upon thermomechanical relaxation, the atoms in Vitreloy 4 decompose into clusters with local atomic density fluctuation. Both the time scale of the decomposition process and the composition difference between the decomposed phases and the nominal composition of the as-received material affect the sequence and extent of the crystallization event(s). It was proposed by Waniuk et al.,[27] in an isothermal annealing study of the Vitreloy 1 to Vitreloy 4 alloy family, that the decomposition process acts as a precursor to crystallization in the case of low-temperature annealing where both primary and secondary crystallizations exist, while it does not influence high-temperature crystallization where only one abrupt crystallization event exists. Analogous to Wainuk's analysis, it appears that during the high-temperature deformation of Vitreloy 4 conducted in this study, mechanical loading at different strain rates introduces structural relaxation in the material that causes different decomposition configurations without necessarily introducing phase separation or nanocrystallization.

B. Free volume change and the effect on flow stress

The hypothesis of free volume in glassy materials was first proposed by Cohen and Turnbull[51] and subsequently

adapted for metallic glasses by Spaepen.[22] Metallic glasses are formed by rapidly quenching metallic melts (liquids) at cooling rates adequate to restrict atomic movement and suppress crystallization. Therefore, a certain number of "holes" or "voids" of various sizes are quenched into the atom clusters that form the amorphous structure. Such "holes" or "voids" are referred to as "free volume," which is suggested to be the key to allow the atomic motion for the diffusive arrangement or ordering of atoms. The possibility of an atom jumping into adjacent holes (free volumes) depends on the relative size of the atoms and the holes. The creation and annihilation of free volume during structural relaxation of amorphous alloys is both a kinetic and a thermodynamic process. With the assumption that the heat release rate of an amorphous material is proportional to the rate of creation of free volume, a group of researchers[7,23,24] studied the free volume evolution during high-temperature deformation and concluded that the free volume increases with strain rate and strain until steady-state flow occurs, which agrees with the experimental observations in this investigation.

Spaepen and Turnbull[22] proposed a flow model to build the correlation of the strain rate, the concentration of flow defects, and the flow stress, which has been widely adopted in analyzing the plastic deformation mechanism of BMGs.

$$\dot{\varepsilon} = 2c_f k_f \frac{\varepsilon_o \nu_o}{\Omega} \sinh\left(\frac{\sigma \varepsilon_o \nu_o}{2k_B T}\right) \quad , \qquad (1)$$

where $\dot{\varepsilon}$ is the strain rate, σ is the uniaxial stress, c_f is the concentration of flow defects, k_f is a rate factor, Ω is the atomic volume, k_B is the Boltzmann's constant, and T is the ambient temperature. In the deformation process, a small amount of volume v_o undergoes a deformation ε_o, the product of which is the activation volume of the process (V_a), which is calculated for both alloys in Sec. IV. C. According to the free volume model by Cohen and Turnbull,[51] the concentration of flow-induced defects results in the accumulation of the excess free volume in the material. It can thereby be inferred from Eq. (1) that the sinh of the flow stress is inversely proportional to the defect concentration at a constant strain rate.

C. Activation volumes for non-Newtonian and Newtonian flow

The results from the successive jump in strain rate tests independently in Newtonian and non-Newtonian regions [Figs. 9(a) and 9(b)] are used to fit the activation volume $\varepsilon_o v_o$ in Eq. (1). The best fits from the free volume model are shown in Figs. 10(a)–10(d) for Vitreloy 1 and Vitreloy 4, both in the non-Newtonian regime [Figs. 10(a) and 10(c)] and in the Newtonian regime [Figs. 10(b) and 10(d)]. The experimental data are shown as solid squares, and the fits of data with Eq. (1) are shown with solid lines. The activation volume $\varepsilon_o v_o (V_a)$ and the prefactor $2k_f c_f \varepsilon_o v_o \Omega^{-1}$ are taken as fitting parameters. The best-fitting parameters are calculated for each set of data and are shown in Table III. Even though it is feasible to fit the data in both Non-Newtonian and Newtonian regimes to obtain the activation volumes for Vitreloy 1 and Vitreloy 4 respectively, as listed in Table III, the underlying changes causing a deviation from Newtonian flow are not clear in such an approach. For the free volume model, the important relevant term is $\sinh[(\sigma\varepsilon_o v_o)/(2k_B T)]$. In general, $\sinh(x) \approx x$ for $x < 1$ and $\sinh(x) \approx (e^x/2)$ for $x > 1$. Thus, Newtonian behavior is expected for $[(\sigma\varepsilon_o v_o)/(2k_B T)] < 1$ and non-Newtonian flow is expected for $[(\sigma\varepsilon_o v_o)/(2k_B T)] > 1$. The present analysis and data shown in Fig. 10 indicate that for both Vitreloy 1 and Vitreloy 4, Newtonian flow is expected at 643 K for stresses less than ~300 MPa for a value of $\varepsilon_o v_o \approx 70$ Å^3, whereas non-Newtonian flow is expected at stresses greater than ~400 MPa for a value of $\varepsilon_o v_o \approx 120$ Å^3. The present analysis therefore provides a basis for rationalizing the transition from Newtonian to non-Newtonian flow in the BMGs.

Spaepen's free volume model has been used by many researchers to determine the activation volume of the deformation process of metallic glasses. For example, Jin et al.[52] performed compression tests on Vit4 specimens pre- or post-heat treated at around the glass transition temperature and calculated the activation volume to be 126 Å^3, which was close to the activation volume of the non-Newtonian flow in current study. The activation volume of $Pd_{41}Ni_{10}Cu_{29}P_{20}$ was found to range between 141 and 152 Å^3 by Heggen et al.[34] by constant true stress creep test on specimen annealed at different elevated temperatures of 550, 555, and 565 K. All these previous approaches did not differentiate the Newtonian and non-Newtonian flow natures of the homogeneous plastic deformation of metallic glass. This is the first study to reveal the difference between Newtonian and non-Newtonian flow in terms of the activation volume. The much smaller activation volume in Newtonian flow, for both Vitreloy 1 and Vitreloy 4, is associated with higher diffusibility and atomistic mobility of the free volume in the material. Similarly, the activation volumes are smaller in Vitreloy 4

TABLE III. Activation volume and prefactor in the free volume model [Eq. (1)] from the result of multiple strain rate jump tests modeled in Fig. 10.

Material	$V_a = \varepsilon_o v_o$ (Å^3)	$2k_f c_f \varepsilon_o v_o \Omega^{-1}$ (s^{-1})
Vit1, non-Newtonian	123.7	5.34e−4
Vit1, Newtonian	70.5	1.67e−3
Vit1, all data	111.8	8.30e−4
Vit4, non-Newtonian	115.8	1.36e−3
Vit4, Newtonian	69.6	6.01e−3
Vit4, all data	98.4	2.48e−3

samples after both Newtonian and non-Newtonian compression test compared with Vitreloy 1, which suggests a higher local atomistic mobility in Vitreloy 4 and agrees with previous observation from DSC studies.

V. CONCLUSIONS

The high-temperature deformation mechanisms of two amorphous alloys, $Zr_{41.2}Ti_{13.8}Cu_{12.5}Ni_{10}Be_{22.5}$ (Vitreloy 1 or Vit1) and $Zr_{46.8}Ti_{8.2}Cu_{7.5}Ni_{10}Be_{27.5}$ (Vitreloy 4 or Vit4), were studied under uniaxial compression combined with DSC and TEM examination. The following conclusions can be drawn from this investigation:

(1) DSC and TEM/x-ray diffraction examination on Vitreloy 1 and Vitreloy 4 specimens deformed at 643 K and various strain rates reveals different structural relaxation mechanisms in the two material systems. In Vitreloy 1, mechanical loading increases the extent of the spinodal phase separation and reduces the temperature at which it occurs. This phase separation is responsible for nucleating nanocrystallites during the low strain rate tests, which is observed with both TEM and x-ray diffraction in this study. In Vitreloy 4, no such phase separation is discerned from the DSC traces and no crystallization is observed under TEM and x-ray diffraction spectra. Decomposition in the form of local chemical composition fluctuation dominates and has a strong influence in the deformation tests performed at relatively high strain rates. Such influence is small when the material is compressed at a much lower strain rate since the material has enough time to relax to a more stable configuration.

(2) The different relaxation mechanisms in Vitreloy 1 and Vitreloy 4 result in changes in the free volume in the material following deformation. The amount of free volume in Vitreloy 1 does not show noticeable change after either constant strain rate or jump in strain rate deformation. For Vitreloy 4, the specimen subjected to jump in strain rate accumulated certain amount of free volume during the high strain rate portion of the deformation. Because additional free volume is associated with lower flow stress at a given strain rate, the Vitreloy 4 specimen subjected to the jump in strain rate test loses two-thirds of its flow stress (strength) compared with a sample deformed at a corresponding constant strain rate. A Vitreloy 1 specimen subjected to jump in strain rate has almost identical flow stress after the drop in strain rate as a sample subjected to the corresponding constant strain rate, as there is no difference in the free volume in these specimens.

(3) The activation volumes of non-Newtonian flow and Newtonian flow for Vitreloy 1 and Vitreloy 4 were calculated from the results of successive strain rate jump tests. The activation volume of the Newtonian flow is found to be much smaller than that of the non-Newtonian flow for both Vitreloy 1 and Vitreloy 4. Smaller activation volumes in Vitreloy 4 compared with those of Vitreloy 1 in both Newtonian and non-Newtonian flows suggests that Vitreloy 4 has higher atomistic mobility than Vitreloy 1.

ACKNOWLEDGMENTS

The research reported here was supported by the National Science Foundation MRSEC Program by a grant (No. 0520565) to the Center for Science and Engineering of Materials at the California Institute of Technology and is gratefully acknowledged. The authors thank Mr. Petros Arakelian for his help with the mechanical testing.

REFERENCES

1. W. Klement, R.H. Willens, and P. Duwez: Non-crystalline structure in solidified gold-silicon alloys. *Nature* **187,** 869 (1960).
2. W.L. Johnson: Metastable phases, in *Intermetallic Compounds*, Vol. 1 (Wiley, New York, 1994), p. 687.
3. J. Lu, G. Ravichandran, and W.L. Johnson: Deformation behavior of the $Zr_{41.2}Ti_{13.8}Cu_{12.5}Ni_{10.0}Be_{22.5}$ bulk metallic glass over a wide range of strain-rates and temperatures. *Acta Mater.* **51,** 3429 (2003).
4. T.G. Nieh, J. Wadsworth, J.C.T. Liu, T. Ohkubo, and Y. Hirotsu: Plasticity and structural instability in a bulk metallic glass deformed in the supercooled liquid region. *Acta Mater.* **49,** 2887 (2001).
5. Y. Kawamura, T. Shibata, A. Inoue, and T. Masumoto: Deformation behavior of $Zr_{65}Al_{10}Ni_{10}Cu_{15}$ glassy alloy with wide supercooled liquid region. *Appl. Phys. Lett.* **69,** 1208 (1996).
6. T.G. Nieh, C. Schuh, J. Wadsworth, and Y. Li: Strain rate-dependent deformation in bulk metallic glasses. *Intermetallics* **10,** 1177 (2002).
7. B. van Aken, P. de Hey, and J. Sietsma: Structural relaxation and plastic flow in amorphous $La_{50}Al_{25}Ni_{25}$. *Mater. Sci. Eng., A* **278,** 247 (2000).
8. A. Inoue, B. Shen, and C. Chang: Super-high strength of over 4000 MPa for Fe-based bulk glassy alloys in $[(Fe_{1-x}Co_x)_{0.75}B_{0.2}Si0_{.059}]_{96}Nb_4$ system. *Acta Mater.* **52,** 4093 (2004).
9. A. Inoue, B.L. Shen, A.R. Yavari, and A.L. Greer: Mechanical properties of Fe-based bulk glassy alloys in Fe–B–Si–Nb and Fe–Ga–P–C–B–Si systems. *J. Mater. Res.* **18,** 1487 (2003).
10. N. Nishiyama and A. Inoue: Glass-forming ability of bulk $Pd_{40}Ni_{10}Cu_{30}P_{20}$ alloy. *Mater. Trans., JIM* **37,** 1531 (1996).
11. H. Kato, Y. Kawamura, A. Inoue, and H.S. Chen: Newtonian to non-Newtonian master flow curves of a bulk glass alloy $Pd_{40}Ni_{10}Cu_{30}P_{20}$. *Appl. Phys. Lett.* **73,** 3665 (1998).
12. J.S. Harmon, M.D. Demetriou, W.L. Johnson, and M. Tao: Deformation of glass forming metallic liquids: Configurational changes and their relation to elastic softening. *Appl. Phys. Lett.* **90,** 131912 (2007).
13. C.A. Schuh, T.C. Hufnagel, and U. Ramamurty: Mechanical behavior of amorphous alloys. *Acta Mater.* **55,** 4067 (2007).
14. A.S. Argon: Plastic deformation in metallic glasses. *Acta Metall.* **27,** 47 (1979).
15. A.S. Argon and L.T. Shi: Development of visco-plastic deformation in metallic glasses. *Acta Metall.* **31,** 499 (1983).
16. H. Kato, Y. Kawamura, H.S. Chen, and A. Inoue: A fictive stress model calculation of nonlinear viscoelastic behaviors in a

Zr-based glassy alloy: Stress growth and relaxation. *Jpn J. Appl. Phys., Part 1* **39,** 5184 (2000).
17. V.A. Khonik: The kinetics of irreversible structural relaxation and homogeneous plastic flow of metallic glasses. *Phys. Status Solidi A* **177,** 173 (2000).
18. W.L. Johnson and K. Samwer: A universal criteria for plastic yielding of metallic glasses with a $(T/Tg)^{2/3}$ temperature dependence. *Phys. Rev. Lett.* **95,** 195501 (2005).
19. M.L. Lind, G. Duan, and W.L. Johnson: Isoconfigurational elastic constants and liquid fragility of a bulk metallic glass forming alloy. *Phys. Rev. Lett.* **97,** 015501 (2006).
20. M.D. Demetriou, J.S. Harmon, M. Tao, G. Duan, K. Samwer, and W.L. Johnson: Cooperative shear model for the rheology of glass-forming metallic liquids. *Phys. Rev. Lett.* **97,** 065502 (2006).
21. G. Duan, M.L. Lind, M.D. Demetriou, W.L. Johnson, W.A. Goddard III, T. Cagin, and K. Samwer: Strong configurational dependence of elastic properties for a binary model metallic glass. *Appl. Phys. Lett.* **89,** 151901 (2006).
22. F. Spaepen and D. Turnbull: A mechanism for the flow and fracture of metallic glasses. *Scr. Metall. Mater.* **8,** 563 (1974).
23. P.A. Duine, J. Sietsma, and A. Van den Beukel: Characterization of free volume in atomic models of metallic glasses. *Acta Metall. Mater.* **40,** 743 (1992).
24. P. de Hey, J. Sietsma, and A. Van den Beukel: Structural disordering in amorphous $Pd_{40}Ni_{40}P_{20}$ induced by high temperature deformation. *Acta Mater.* **46,** 5873 (1998).
25. L. Anand and C. Su: A theory for amorphous viscoplastic materials undergoing finite deformations with application to metallic glasses. *J. Mech. Phys. Solids* **53,** 1362 (2005).
26. L. Anand and C. Su: A constitutive theory for metallic glasses at high homologous temperatures. *Acta Mater.* **55,** 3735 (2007).
27. T. Waniuk, J. Schroers, and W.L. Johnson: Timescales of crystallization and viscous flow of the bulk glass-forming Zr–Ti–Ni–Cu–Be alloys. *Phys. Rev. B* **67,** 184203 (2003).
28. E. Pekarskaya, J.F. Loffler, and W.L. Johnson: Microstructural studies of crystallization of a Zr-based bulk metallic glass. *Acta Mater.* **51,** 4045 (2003).
29. H. Chen, Y. He, G.J. Shiflet, and S.J. Poon: Deformation-induced nanocrystal formation in shear bands of amorphous-alloys. *Nature* **367,** 541 (1994).
30. M.C. Gao and R.E. Hackenberg: Deformation-induced nanocrystal precipitation in Al-base metallic glasses. *Mater. Trans.* **42,** 1741 (2001).
31. J.J. Kim, Y. Choi, S. Suresh, and A.S. Argon: Nanocrystallization during nanoindentation of a bulk amorphous metal alloy at room temperature. *Science* **295,** 654 (2002).
32. W.H. Jiang, F.E. Pinkerton, and M. Atzmon: Deformation-induced nanocrystallization: A comparison of two amorphous Al-based alloys. *J. Mater. Res.* **20,** 696 (2005).
33. M. Heggen, F. Spaepen, and M. Feuerbacher: Plastic deformation of $Pd_{41}Ni_{10}Cu_{29}P_{20}$ bulk metallic glass. *Mater. Sci. Eng., A* **375,** 1186 (2004).
34. M. Heggen, F. Spaepen, and M. Feuerbacher: Creation and annihilation of free volume during homogeneous flow of a metallic glass. *J. Appl. Phys.* **97,** 033506 (2005).
35. T.G. Nieh, T. Mukai, and C.T. Liu: Superplastic behavior of a Zr–10Al–5Ti–17.9Cu–14.6Ni metallic glass in the supercooled liquid region. *Scr. Mater.* **40,** 1021 (1999).
36. T.G. Nieh, J. Wadsworth, C.T. Liu, G.E. Ice, and K.S. Chung: Extended plasticity in the supercooled liquid region of bulk metallic glasses. *Mater. Trans.* **42,** 613 (2001).
37. S. Schneider, P. Thiyagarajan, and W.L. Johnson: Formation of nanocrystals based on decomposition in the amorphous $Zr_{41.2}Ti_{13.8}Cu_{12.5}Ni_{10}Be_{22.5}$ alloy. *Appl. Phys. Lett.* **68,** 493 (1996).
38. R. Busch, S. Schneider, A. Peker, and W.L. Johnson: Decomposition and primary crystallization in undercooled $Zr_{41.2}Ti_{13.8}Cu_{12.5}Ni_{10.0}Be_{22.5}$ melts. *Appl. Phys. Lett.* **67,** 1544 (1995).
39. K.F. Kelton, T.K. Croat, A.K. Gangopadhyay, L.Q. Xing, A.L. Greer, M. Weyland, X. Li, and K. Rajan: Mechanisms for nanocrystal formations in metallic glasses. *J. Non-Cryst. Solids* **317,** 71 (2003).
40. A. Peker and W.L. Johnson: A highly processable metallic-glass—$Zr_{41.2}Ti_{13.8}Cu_{12.5}Ni_{10.0}Be_{22.5}$. *Appl. Phys. Lett.* **63,** 2342 (1993).
41. R. Busch, Y.J. Kim, and W.L. Johnson: Thermodynamics and kinetics of the undercooled liquid and the glass transition of the $Zr_{41.2}Ti_{13.8}Cu_{12.5}Ni_{10.0}Be_{22.5}$ alloy. *J. Appl. Phys.* **77,** 4039 (1995).
42. R. Busch, E. Bakke, and W.L. Johnson: Viscosity of the supercooled liquid and relaxation at the glass transition of the $Zr_{46.75}Ti_{8.25}Cu_{7.5}Ni_{10}Be_{27.5}$ bulk metallic glass forming alloy. *Acta Mater.* **46,** 4725 (1998).
43. K. Samwer, R. Busch, and W.L. Johnson: Change of compressibility at the glass transition and prigogine-defay ratio in ZrTiCuNiBe alloys. *Phys. Rev. Lett.* **82,** 580 (1999).
44. N. Van Steenberge, A. Concustell, J. Sort, J. Dasc, N. Mattern, A. Gebert, S. Suriñach, J. Eckert, and M.D. Baró: Microstructural inhomogeneities introduced in a Zr-based bulk metallic glass upon low-temperature annealing. *Mater. Sci. Eng., A* **491,** 124 (2008).
45. I. Martin, T. Ohkubo, M. Ohnuma, B. Deconihout, and K. Hono: Nanocrystallization of $Zr_{41.2}Ti_{13.8}Cu_{12.5}Ni_{10.0}Be_{22.5}$ metallic glass. *Acta Mater.* **52,** 4427 (2004).
46. T.G. Nieh, C. Iwamoto, Y. Ikuhara, K.W. Lee, and Y.W. Chung: Comparative studies of crystallization of a bulk Zr–Al–Ti–Cu–Ni amorphous alloy. *Intermetallics* **12**(11), 1183 (2004).
47. D. Fatay, J. Gubicza, P. Szommer, J. Lendvai, M. Bletry, and P. Guyot: Thermal stability and mechanical properties of a Zr-based bulk amorphous alloy. *Mater. Sci. Eng., A* **387–389,** 1001 (2004).
48. M. Bletry, P. Guyot, Y. Brechet, J.J. Blandin, and J.L. Soubeyroux: Homogeneous deformation of bulk metallic glasses in the supercooled liquid state. *Mater. Sci. Eng., A* **387,** 1005 (2004).
49. Y.L. Gao, J. Shen, J.F. Sun, and G. Wang: Crystallization of Zr–Al–Ni–Cu bulk amorphous alloy during continuous heating. *Rare Met. Mater. Eng.* **32,** 518 (2003).
50. J.F. Loffler and W.L. Johnson: Model for decomposition and nanocrystallization of deeply undercooled $Zr_{41.2}Ti_{13.8}Cu_{12.5}Ni_{10}Be_{22.5}$. *Appl. Phys. Lett.* **76,** 3394 (2000).
51. M.H. Cohen and D. Turnbull: Molecular transport in liquids and glasses. *J. Chem. Phys.* **31-5,** 1164 (1959).
52. H.J. Jin, P. Wen, and K. Lu: Pressure effect on glass transition in a $Zr_{65}Al_{7.5}Cu_{27.5}$ metallic glass. *Appl. Phys. Lett.* **83,** 3284 (2003).